crystals

MDPI

Article

Field-Induced Magnetic Phase Transitions and Rich Phase Diagram of $HoMnO_3$ Single Crystal

Chao Dong, Rui Chen *, Yongjie Liu, Congbin Liu, Haipeng Zhu, Jiezun Ke, Wanxin Liu, Ming Yang and Junfeng Wang *

Wuhan National High Magnetic Field Center and School of Physics, Huazhong University of Science and Technology, Wuhan 430074, China

* Correspondence: r-cheng@foxmail.com (R.C.); jfwang@hust.edu.cn (J.W.); Tel.: +86-027-87792333 (R.C. & J.W.)

Received: 24 July 2019; Accepted: 12 August 2019; Published: 13 August 2019

Abstract: An extensive magnetization study in pulsed fields up to 62 T and at temperatures down to ~0.7 K has been performed on the single crystals of hexagonal manganite $HoMnO_3$. For magnetic fields (H) applied along the c-axis, successive magnetic transitions below 10 T and a step-like transition at ~41 T are observed. The phase diagram for $H//c$ is very complex and new phase boundaries are explored below 6 K. This phase diagram is compared with the early results derived from dielectric constant and neutron scattering measurements. For $H//a$, two magnetic transitions are found below 3 T dome-shaped and the phase diagram is reported for the first time. The variety of magnetic symmetries of the field-induced magnetic phases is discussed.

Keywords: hexagonal manganite; magnetic transition; phase diagram; magnetic symmetry

1. Introduction

Field-induced magnetic phase transition, characterized as a change in magnetization, is a long-standing issue of magnetic materials [1]. Of particular interest are the highly frustrated hexagonal (h-) manganites $RMnO_3$ (R = Ho-Lu, Y, Sc), which exhibit phase transitions at low temperature (T) and in the applied magnetic field (H) [2]. Among them, h-$HoMnO_3$ is the most studied compound due to its multiferroic property and rich H-T phase diagram [2–4]. Figure 1a shows the crystallographic structure of h-$HoMnO_3$ with magnetic ions of Mn^{3+} and Ho^{3+}. The Mn^{3+} ions form triangular layers stacked along the c-axis, whereas the Ho^{3+} ions are situated at two different sites 2a and 4b between the layers. As T is lowered, h-$HoMnO_3$ undergoes three phase transitions at T_N = 76 K, T_{SR} = 32.8 K, and T_{Ho} = 5.4 K, respectively [2]. The phase diagram of h-$HoMnO_3$ for H along the c-axis is extremely complex for H < 8 T. Three magnetic ordered phases (HT1, HT2, and INT) were identified above 5 K, whereas below this temperature more phases and phase boundaries were explored by means of different experimental techniques [5–11]. Through dielectric constant measurements, Yen et al. observed two dome-shaped phases (LT1, LT2) and additional boundaries in the INT phase [6]. Similar results were obtained by measurements of susceptibility, specific heat, microwave, and ultrasonic velocity [7–9]. However, the neutron scattering experiments revealed different phase diagrams in the ranges of 0–5 K and 0–2 T; four boundaries merge into a multicritical point (7 K, 1.4 T) and no LT1 phase was observed [10,11]. On the other hand, the determination of the magnetic structures of these phases is challenging because of the large unit cell and the complexity of this spin system. By optical second harmonic generation (SHG), Fiebig et al. studied the change in symmetry of the Mn^{3+} ions above 5 K [12,13]. However, magnetic symmetries of the LT1, LT2 phases, as well as the magnetic ground state still remain puzzling [2,14]. In addition, the variety of symmetries of the Ho^{3+} ions, which orient along the c-axis, is rarely studied [15]. These controversial results and questions

motivate a reinvestigation of the field-induced magnetic transitions and phase diagram of *h*-$HoMnO_3$ using other experimental techniques.

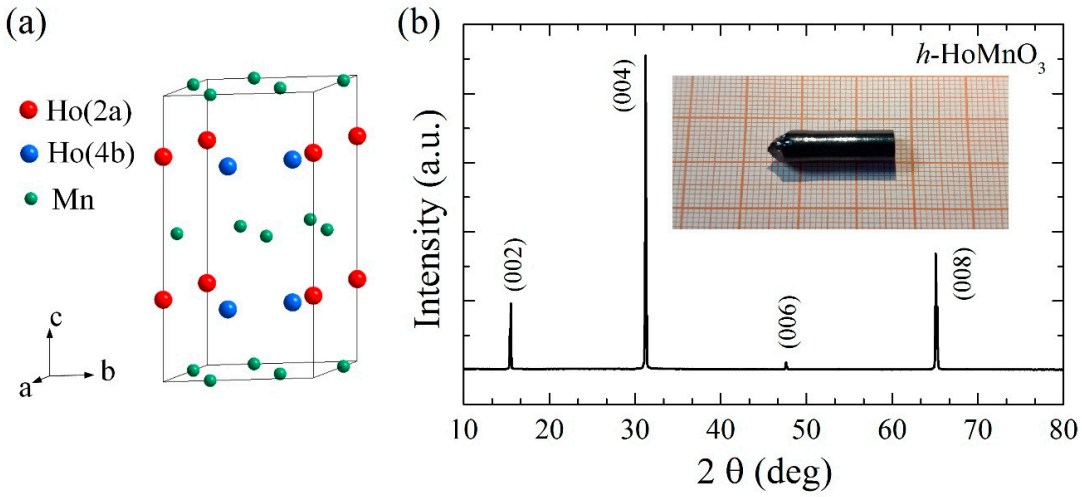

Figure 1. (**a**) Crystallographic geometry of the Mn^{3+} and Ho^{3+} ions in the *h*-$HoMnO_3$. Two nonequivalent Ho^{3+} ions 2*a* and 4*b* are shown in different colors. (**b**) The orientation of the crystal surface using X-ray scattering analysis for the (002) plane. Inset of Figure 2 shows a picture of the as-grown *h*-$HoMnO_3$ single crystal by the optical floating-zone furnace.

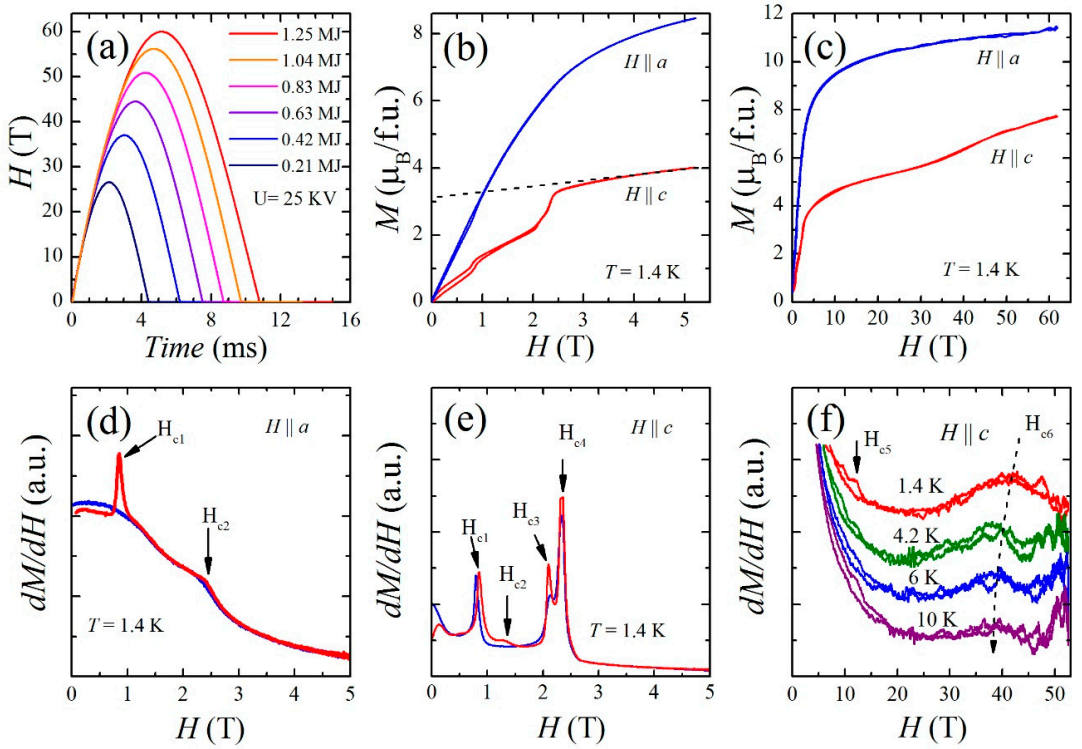

Figure 2. (**a**) Waveforms of pulsed fields driven by various capacitor banks. To generate an 11 ms/62 T pulsed field, a 1.25 MJ capacitor bank with a discharge voltage 25 kV is applied. While the 0.21 MJ capacitor bank is used to generate a ~4 ms short-pulsed field. (**b**) Magnetization data measured at 1.4 K for *H*//*a* and *H*//*c*, respectively. The data were measured using a ~4 ms short-pulsed field. The dashed line shows linearly extrapolating the magnetization data to zero fields. (**c**) A comparison between the *a*- and *c*-axis magnetizations in fields up to 62 T. (**d**,**e**) The derivative d*M*/d*H* of the data in (**b**). The red (blue) curve denotes the field-increasing (-decreasing) process. (**f**) The derivative d*M*/d*H* of the data in (**c**). The arrows in (**d**–**f**) indicate the field-induced magnetic phase transitions.

Magnetization (M) measurement using a non-destructive pulsed magnet can explore phase transition in a sufficiently high magnetic field. Due to its fast field-sweeping rate (> 1 kT/s) and high-speed (60 MS/s) data collection system, this induction method using a compensated pickup coil is also utilized to detect weak magnetic transition, which is not clearly shown in a steady field. In this work, we measure the magnetization of h-$HoMnO_3$ in a pulsed-field up to 62 T and explore a new transition at ~41 T for $H//c$. The pulsed duration is shorter and the sensitivity of the coil is higher. By using a short-pulsed field of ~4 ms and measurement down to ~0.7 K, we reinvestigate the c-axis magnetic transitions and phase diagram below 5 T. Possible magnetic structures and symmetries of the Ho^{3+} ions are proposed for the field-induced magnetic phases. For $H//a$, two new magnetic transitions are observed below 5 T and the phase diagram is reported.

2. Experimental Details

Single crystals of h-$HoMnO_3$ were grown by the floating zone method. First, the polycrystalline powder of h-$HoMnO_3$ was synthesized by the conventional solid-state reaction. Stoichiometric mixtures of Ho_2O_3 and Mn_2O_3 powders were ground and sintered in air at 1120 °C for 24 h. This process was repeated for several times to ensure fully reaction of the starting materials. Then the product was pressed into ~10 cm long rods under a 50 MPa hydrostatic pressure. The rods were sintered at 1120 °C for 20 h and used as feed rod and seed rod. The single crystal growth was then carried out using an optical floating-zone furnace (FZ-T-10000-H, Crystal System Incorporation of Japan). The experimental conditions are almost the same as those in Ref. [16]. The inset of Figure 1b shows the as-grown h-$HoMnO_3$ single crystal with a diameter of ~7 mm. The crystal was oriented by the X-ray single-crystal diffractometer (XtaLAB mini™ II, Rigaku, Japan), examined by an X-ray powder diffractometer (XRD, Philips X'pert pro, Japan) as shown in Figure 1b and found to have good quality.

Magnetization measurement was performed in Wuhan National High Magnetic Field Center using a 65 T pulsed magnet. Figure 2a shows the pulsed fields with a discharge voltage of 25 kV driven by different capacitor banks. The pulse duration can be controlled from ~4 ms to 11 ms with peak field changing from 25 to 60 T. In the experiment, two pulse shots with sample-in and sample-out were carried out to subtract the spurious dB/dt signals induced by the pulsed fields. dM/dt signals from the sample were then collected and integrated as a function of magnetic fields. The absolute value of the magnetization was obtained by a comparison with the data measured by a commercial superconducting quantum interference device (SQUID, Quantum Design). He-3 cryogenic system was employed for the measurements down to ~0.7 K.

3. Results and Discussion

Figure 2b shows the magnetization processes of h-$HoMnO_3$ at 1.4 K and in a pulsed-field up to 5 T. For $H//a$, the M increases monotonously with a bend in the vicinity of 3 T. From the derivative dM/dH shown in Figure 2d, we distinguish two magnetic transitions at H_{c1} = 1 T and H_{c2} = 2.5 T. The H_{c1} transition was not detected in the previous work [17], probably due to the relatively slow field-sweeping rate. A hysteresis is seen around H_{c1}, indicating the nature of a first-order transition. For $H//c$, clear magnetization jumps are seen at ~1 T and ~2.5 T. The dM/dH data in Figure 2e show four successive magnetic transitions at H_{c1} = 0.8 T, H_{c2} = 1.4 T, H_{c3} = 2 T, and H_{c4} = 2.4 T, in agreement with the result in Ref. [18]. Because the H_{c2} transition is of the first-order type [18], it gives rise to the hysteresis in a pulsed field below 1.5 T. In higher magnetic fields up to 62 T [Figure 2c], the magnetization for $H//c$ shows a change of slope at ~10 T followed by another step-like transition at ~41 T. These two anomalies (H_{c5}, H_{c6}) are also visible in dM/dH curves, as shown in Figure 2f. While for $H//a$, no transition is observed and the magnetization almost saturates above 10 T.

We first study the magnetic transitions for $H//a$. Figure 3a shows the dM/dH curves from 0.73 to 5 K. It is found that both H_{c1} and H_{c2} develop well with the temperature and almost disappear at 5 K. The corresponding phase boundaries are shown in the phase diagram of Figure 3b, which was not reported previously. When T is further increased, the two boundaries seem to end at the transition

temperature of T_{Ho} (5.4 K) at H = 0 T because the other two transitions (T_{SR} and T_N) appear at much higher temperatures of 32.8 and 76 K, respectively. It is known that the Mn^{3+} spins strictly orient in the *ab* plane, whereas the Ho^{3+} spins are mainly aligned along the *c*-axis due to a strong uniaxial anisotropy [2,13]. Therefore, we attribute the two transitions in Figure 3a to the magnetic reorientation of the Mn^{3+} spins in applied *a*-axis fields. As determined by the SHG experiment [13], magnetic symmetries of the two phases above and below T_{Ho} are $P\underline{6}_3c\underline{m}$ (Γ_3) and $P6_3cm$ (Γ_1), respectively. Since no other transition is observed above T_{Ho} by our magnetization data, the symmetry of the high-field phase should be the same as the high-temperature phase, i.e., $P\underline{6}_3c\underline{m}$. For the middle phase between H_{c1} and H_{c2}, however, the magnetic symmetry is not clear at the moment. Interestingly, we find that the two transition fields are approximate to those of the magnetization jumps for $H//c$. Whether it is an intermediate phase ($P\underline{6}_3$) or not as observed for $H//c$ needs further investigation.

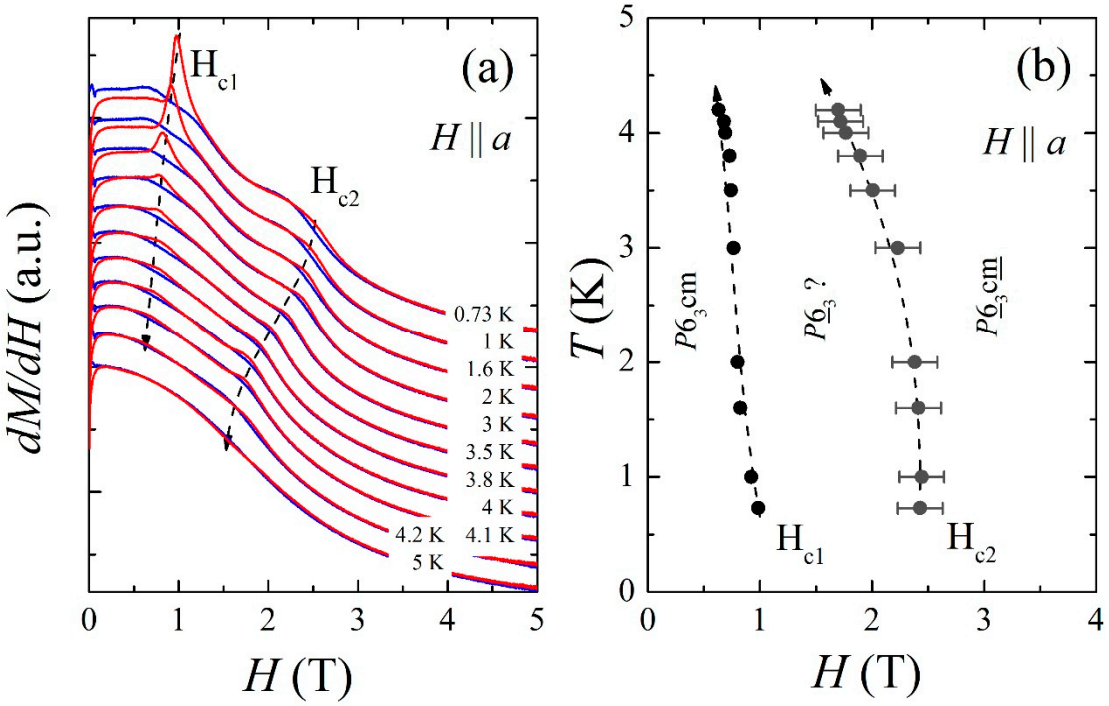

Figure 3. (**a**) d*M*/d*H* curves measured from 5 to 0.73 K for *H*//*a*. The red (blue) curve is for the increasing (decreasing) field. (**b**) *H*-*T* phase diagram for *H*//*a*. The error bar indicates the broad peak at H_{c2}. The dashed lines are guided for eyes.

The most important feature of *h*-$HoMnO_3$ is the successive magnetic transitions for *H*//*c*. We performed comprehensive magnetization measurements at temperatures from 45 down to 0.77 K. The derivative d*M*/d*H* data are shown in Figure 4a,b. There is a little difference in the low-temperature region between the data of *H*-increasing and -decreasing processes. It is ambiguous that the evolutions of H_{c1} are opposite and H_{c2} is almost invisible in the decreasing field. At temperatures above 6 K, the d*M*/d*H* curve shows a plateau, which moves firstly to the high field and then to the low field, as indicated by the dashed lines. From the d*M*/d*H* anomalies, we summarize the *H*-*T* phase diagram of *H*//*c* in Figure 4c. At a first glance, a dome-shaped phase ($P\underline{6}_3c\underline{m}$) below 43 K and an intermediate phase ($P\underline{6}_3$) in a higher field are demonstrated, which are consistent with all early results [5–12]. Note that the phase boundary at 5 K and 0–1 T is not observed in this study. The reason is that this boundary is nearly temperature independent and thus insensitive to our measurement. Upon a close inspection on the low-*T* region, it looks different from those reported in Refs. [6–9], but similar to the result derived from the neutron scattering experiment [10,11]. Below 5 K, three phases labeled as I, II, and III appear between H_{c1} and H_{c4}. The puzzling LT1 and LT2 phases determined by a dielectric constant are not observed in our data. Besides, the dielectric constant and susceptibility measurements revealed

that H_{c3} and H_{c4} merged into one multicritical point at 1.4 K [2,7]. However, these two transitions, associated with a critical endpoint at 2.05 T and 2.2 K [18], can be distinguished in our data even down to 0.77 K. Another interesting finding in Figure 4c is the evolution of the H_{c3} transition. From the neutron scattering data, Vajk et al. proposed a boundary extending H_{c3} to a multicritical point at 7 K and 1.4 T [10,11]. However, this transition seems to end at 3.5 K and 2.5 T, where a first-order transition appears and separates phases II and III from the intermediate phase. It is noteworthy that similar hysteresis effect was observed in the same area by the dielectric constant measurement [6].

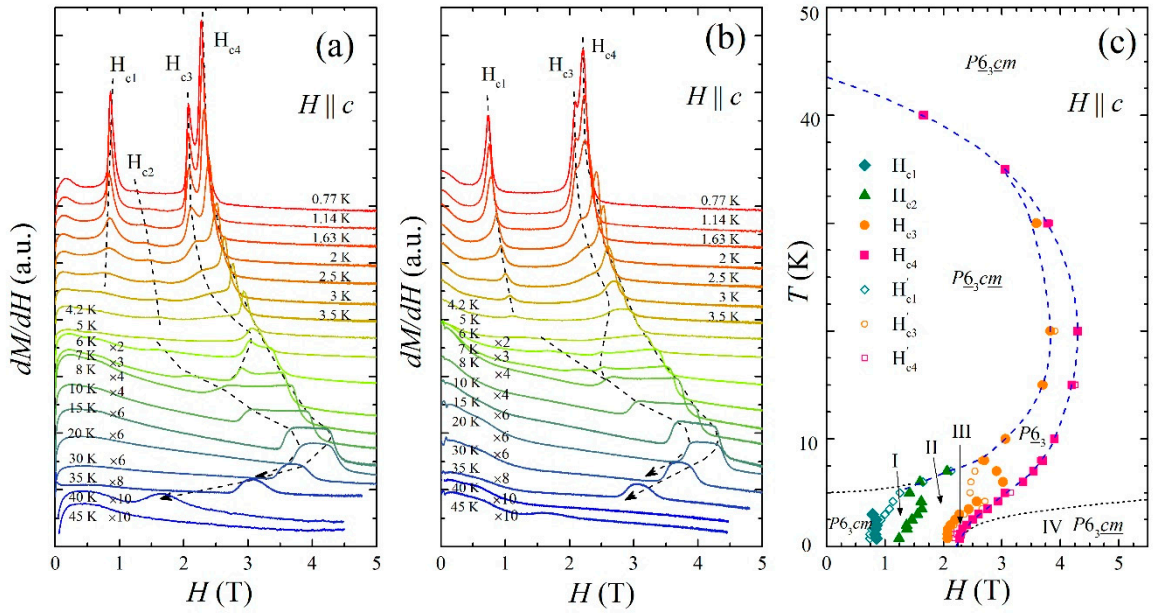

Figure 4. d*M*/d*H* curves for *H*//*c* measured from 45 to 0.77 K. For clarity, the data for increasing and decreasing fields are shown in (**a**) and (**b**), respectively. Dashed lines are guided for eyes. (**c**) The resulting *H*-*T* phase diagram for *H*//*c*. Phases I-III are the result in this work, while phase IV and the phase boundaries (dotted lines) show the result obtained in Ref. [8]. The hysteresis effect is observed between phase II and the $P6_3$ phase. The change of magnetic symmetry is discussed in the text.

To understand the *H*//*c* phase diagram, the role of the Ho^{3+} spins and their interaction with the Mn^{3+} spins should be considered. In a zero field, the Ho^{3+} spins undergo a change of magnetic symmetry from $P\underline{6}_3\underline{c}m$ to $P\underline{6}_3c\underline{m}$ ($\Gamma_4 \rightarrow \Gamma_3$) at T_{SR} and then another change from $P\underline{6}_3c\underline{m}$ to $P6_3cm$ ($\Gamma_3 \rightarrow \Gamma_1$) at T_{Ho} [10,15]. While following neutron experiment did not find a transition at T_{Ho} arising from the Ho^{3+} orderings [14]. For $P\underline{6}_3c\underline{m}$, all the Ho^{3+} spins are ordered along the *c*-axis. Due to a strong uniaxial anisotropy, it is hard to align the Ho^{3+} spins along the *a*-axis by magnetic fields. However, as shown in Figure 2c, the magnetic moment for *H*//*a* quickly reaches ~9 μ_B/f.u. at 5 T, much larger than the saturation moment (4.9 μ_B) of the Mn^{3+} spins. In the case of $P6_3cm$, the Ho^{3+} spins are disordered and may contribute to a rapid increase in the *a*-axis magnetization, in agreement with our magnetization data. In Figure 2c, the magnetic moment for *H*//*c* is smaller than that for *H*//*a*. This is because the Mn^{3+} spins lying in the *ab* plane do not contribute much to the *c*-axis magnetization. For *H*//*c*, the H_{c3} and H_{c4} transitions are accompanied by a large magnetization jump, see Figure 2b. By extrapolating the magnetization data above H_{c4} to zero fields, the magnetic moment at 0 T is ~3.1 μ_B, which is nearly 1/3 of the effective moment of Ho^{3+} (10.4 μ_B). Given the four allowed symmetries (Γ_1–Γ_4) of Ho^{3+}, only Γ_2 ($P6_3\underline{c}m$) can realize, such a ferrimagnetic phase. This scenario is similar to the 1/3-magnetization plateau phase in the analog *h*-$RMnO_3$ (*R* = Er, Yb) [19]. Based on the above analysis, the variety of Ho^{3+} spin structures in applied fields is proposed in Figure 5. The H_{c5} transition is characterized by other techniques, such as thermal conductivity [17]. A flip of the Ho^{3+} 2*a* spins at H_{c6} coincides with a step-like transition at ~41 T. The reorientation of spins around H_{c6} is not continuous, while it will be continuous above this transition in a higher field. The magnetic structures of phase

I–III in Figure 4c remain unclear, which are likely a result of the rotation of the Mn^{3+} spins triggered by a mutual induction of the Ho^{3+} and Mn^{3+} moments [18].

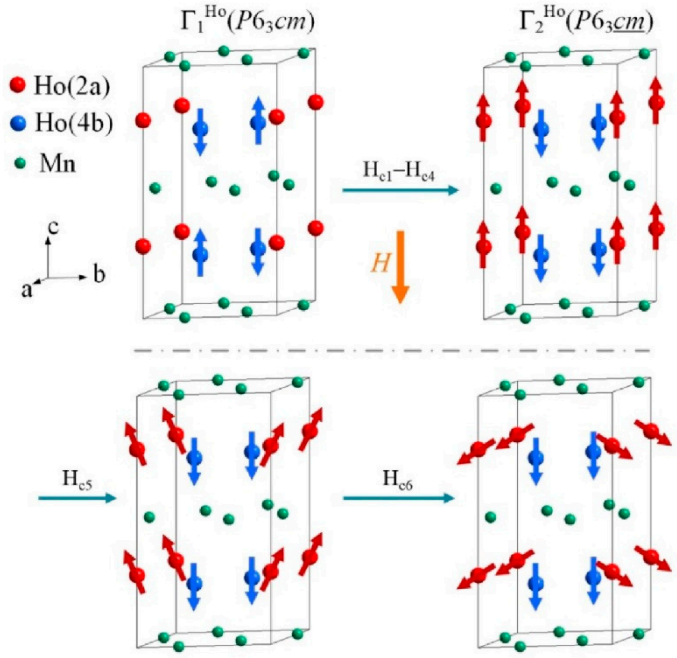

Figure 5. Proposed magnetic structures of the Ho^{3+} 2*a* and 4*b* lattices in applied *c*-axis magnetic fields. The Mn^{3+} spins are not shown because they strictly lie in the *ab* plane.

4. Summary

Large-sized *h*-$HoMnO_3$ single crystals were grown by the optical floating zone method. Magnetization measurements up to 62 T show six magnetic transitions for *H*//*c* and two magnetic transitions for *H*//*a*. By measurements down to ~0.7 K, we construct the phase diagrams of *h*-$HoMnO_3$ for *H*//*a* and *H*//*c*, respectively. The variety of the magnetic symmetry of these field-induced phases is also discussed. The obtained phase diagram for *H*//*c* is very complex, which makes new insight into those results reported previously.

Author Contributions: Y.L. and W.L. grew the crystals by optical floating zone furnace. R.C. and C.L. oriented the crystals by X-ray single-crystal diffraction and cut the samples. C.D., Y.L., and M.Y. conducted the pulsed-field measurements. H.Z. and J.K. help with the He-3 cryogenic system. C.D., R.C., and J.W. analyzed the data and wrote the manuscript.

Acknowledgments: This work was supported by the National Natural Science Foundation of China (11574098 and U1832214), the Fundamental Research Funds for the Central Universities (2018KFYXKJC005) and the National Key R&D Program of China (2016YFA0401704).

Conflicts of Interest: The authors declare no conflict of interest.

References

1. Kindo, K.; Motokawa, M.; De Boer, F. Field-induced magnetic phase transitions. In *High Magnetic Fields: Science and Technology: Theory and Experiments II*; World Scientific: River Edge, NJ, USA, 2006; Volume 3, pp. 125–148.
2. Lorenz, B. Hexagonal manganites-($RMnO_3$): Class (I) multiferroics with strong coupling of magnetism and ferroelectricity. *ISRN Condens. Matter Phys.* **2013**. [CrossRef]
3. Hur, N.; Jeong, I.; Hundley, M.; Kim, S.; Cheong, S.-W. Giant magnetoelectric effect in multiferroic $HoMnO_3$ with a high ferroelectric transition temperature. *Phys. Rev. B* **2009**, *79*, 134120. [CrossRef]
4. Yen, F.; Dela Cruz, C.; Lorenz, B.; Galstyan, E.; Sun, Y.; Gospodinov, M.; Chu, C. Magnetic phase diagrams of multiferroic hexagonal $RMnO_3$ (R = Er, Yb, Tm, and Ho). *J. Mat. Res.* **2007**, *22*, 2163–2173. [CrossRef]

5. Lorenz, B.; Litvinchuk, A.; Gospodinov, M.; Chu, C. Field-Induced reentrant novel phase and a ferroelectric-magnetic order ooupling in $HoMnO_3$. *Phys. Rev. Lett.* **2004**, *92*, 087204. [CrossRef] [PubMed]
6. Yen, F.; Dela Cruz, C.; Lorenz, B.; Sun, Y.; Wang, Y.; Gospodinov, M.; Chu, C. Low-temperature dielectric anomalies in $HoMnO_3$: The complex phase diagram. *Phys. Rev. B* **2005**, *71*, 180407. [CrossRef]
7. Lorenz, B.; Yen, F.; Gospodinov, M.; Chu, C. Field-induced phases in $HoMnO_3$ at low temperatures. *Phys. Rev. B* **2005**, *71*, 014438. [CrossRef]
8. Lemyre, J.C.; Poirier, M.; Pinsard-Gaudart, L.; Revcolevschi, A. Microwave investigation of the phase diagram of hexagonal multiferroic $HoMnO_3$. *Phys. Rev. B* **2009**, *79*, 094423. [CrossRef]
9. Poirier, M.; Lemyre, J.C.; Lahaie, P.-O.; Pinsard-Gaudart, L.; Revcolevschi, A. Enhanced magnetoelastic coupling in hexagonal multiferroic $HoMnO_3$. *Phys. Rev. B* **2011**, *83*, 054418. [CrossRef]
10. Vajk, O.; Kenzelmann, M.; Lynn, J.; Kim, S.; Cheong, S.-W. Magnetic order and spin dynamics in ferroelectric $HoMnO_3$. *Phys. Rev. Lett.* **2005**, *94*, 087601. [CrossRef] [PubMed]
11. Vajk, O.; Kenzelmann, M.; Lynn, J.; Kim, S.; Cheong, S.-W. Neutron-scattering studies of magnetism in multiferroic $HoMnO_3$. *J. Appl. Phys.* **2006**, *99*, 08E301. [CrossRef]
12. Fiebig, M.; Fröhlich, D.; Kohn, K.; Lottermoser, T.; Pavlov, V.; Pisarev, R. Determination of the magnetic symmetry of hexagonal manganites by second harmonic generation. *Phys. Rev. Lett.* **2000**, *84*, 5620. [CrossRef] [PubMed]
13. Fiebig, M.; Lottermoser, T.; Pisarev, R.V. Spin-rotation phenomena and magnetic phase diagrams of hexagonal $RMnO_3$. *J. Appl. Phys.* **2003**, *93*, 8194–8196. [CrossRef]
14. Brown, P.; Chatterji, T. Neutron diffraction and polarimetric study of the magnetic and crystal structures of $HoMnO_3$ and $YMnO_3$. *J. Phys. Condens. Matter* **2006**, *18*, 10085. [CrossRef]
15. Nandi, S.; Kreyssig, A.; Tan, L.; Kim, J.; Yan, J.; Lang, J.; Haskel, D.; McQueeney, R.; Goldman, A. Nature of Ho magnetism in multiferroic $HoMnO_3$. *Phys. Rev. Lett.* **2008**, *100*, 217201. [CrossRef] [PubMed]
16. Fan, C.; Zhao, Z.; Song, J.; Wu, J.; Zhang, F.; Sun, X. Single crystal growth of the hexagonal manganites $RMnO_3$ (R= rare earth) by the optical floating-zone method. *J. Cryst. Growth* **2014**, *388*, 54–60. [CrossRef]
17. Song, J.; Fan, C.; Zhao, Z.; Zhang, F.; Zhao, J.; Liu, X.; Zhao, X.; Liu, Y.; Wang, J.; Sun, X. Magnetization, specific heat, and thermal conductivity of hexagonal $ErMnO_3$ single crystals. *Phys. Rev. B* **2017**, *96*, 174425. [CrossRef]
18. Choi, Y.J.; Lee, N.; Sharma, P.; Kim, S.; Vajk, O.; Lynn, J.; Oh, Y.; Cheong, S.-W. Giant magnetic fluctuations at the critical endpoint in insulating $HoMnO_3$. *Phys. Rev. Lett.* **2013**, *110*, 157202. [CrossRef]
19. Liu, Y.; Wang, J.; Sun, X.; Zhou, J.-S.; Xia, Z.; Ouyang, Z.; Yang, M.; Liu, C.; Chen, R.; Cheng, J.-G. High-field phase diagram and phase transitions in hexagonal manganite $ErMnO_3$. *Phys. Rev. B* **2018**, *97*, 214419. [CrossRef]